Hindawi
International Journal of Rotating Machinery
Volume 2021, Article ID 5598859, 12 pages
https://doi.org/10.1155/2021/5598859

Research Article

Research and Development of a Small-Scale Icing Wind Tunnel Test System for Blade Airfoil Icing Characteristics

Lei Shi,[1,2] **Fang Feng**,[1] **Wenfeng Guo**,[1] **and Yan Li**[1]

[1]*College of Engineering, Northeast Agricultural University, Harbin 150030, China*
[2]*College of Mechanical and Electrical Engineering, Hebei Normal University of Science and Technology, Qinhuangdao 066000, China*

Correspondence should be addressed to Yan Li; liyanneau@163.com

Received 27 February 2021; Revised 19 April 2021; Accepted 3 May 2021; Published 15 May 2021

Academic Editor: Ion Paraschivoiu

In order to study the icing mechanism and anti-icing technology, a small low-speed reflux icing wind tunnel test system was designed and constructed. The refrigeration system and spray system were added to the small reflux low-speed wind tunnel to achieve icing meteorological conditions. In order to verify the feasibility of the test system, the flow field uniformity, temperature stability, and liquid water content distribution of the test section were tested and calibrated. On this basis, the icing tests of an aluminium cylinder, an NACA0018 airfoil, and an S809 airfoil were carried out, and the two-dimensional ice shape obtained by the test was compared with the two-dimensional ice shape obtained by the numerical simulation software. The results show that in the icing conditions and icing time studied, the parameters of the test system are stable, and the experimental ice shape is consistent with the simulated ice shape, which can meet the needs of icing research.

1. Introduction

Surface icing is a typical natural phenomenon, which can bring many problems in the thermal management of HVAC systems, aviation industries, and power networks during winter time [1]. At present, the research on the icing problem is mainly on the mechanism of surface icing and the method of anti-icing/deicing. The main research methods are theoretical analysis, numerical simulation, and icing wind tunnel test [2–4]. In the research of the theoretical derivation of icing, the numerical simulation development of icing, and the development of anti-icing systems, the icing wind tunnel test data are important for design and verification basis. Therefore, an icing wind tunnel plays an indispensable role in icing research [5].

The icing wind tunnel is based on the conventional wind tunnel, with the addition of a refrigeration system and a spray system to achieve icing weather conditions. According to the construction scale, it can be divided into large icing wind tunnels and small icing wind tunnels. Among them, for typical large icing wind tunnels, such as the NASA Glenn Research Center icing wind tunnel (IRT) [6], the Canadian National Research Center icing wind tunnel (PIWT) [7], and the Italian Aerospace Research Center icing wind tunnel [8], the large icing wind tunnel system is complex and its construction and utilization costs are high. The current stage of surface icing research is mainly focused on verification experiments of icing mechanisms and anti-icing/deicing systems by building small icing wind tunnel test systems. The Iowa State University [9] built a small icing wind tunnel with a size of 0.4 m × 0.4 m, which mainly studied a hybrid anti-icing system combined with electric heating and hydrophobic coating on small blades. Zhang et al. [10] used a closed-loop icing wind tunnel with a diameter of 0.6 m to carry out experimental studies on rotating cone icing. Zhu et al. [11] completed the icing process and tested the bond strength of ice in a wind tunnel with a size of 0.5 m × 0.3 m. Gonzales et al. [12] built a simpler icing wind tunnel at the Kanagawa Institute of Technology in Japan to study solar absorption materials on new superhydrophobic surfaces to improve anti-icing performance. Concordia University [13] built a small reflux icing wind tunnel with a cross section of 0.1 m × 0.1 m to study the anti-icing and deicing performance of a superhydrophobic coating on the wing. Rivero et al. [14]

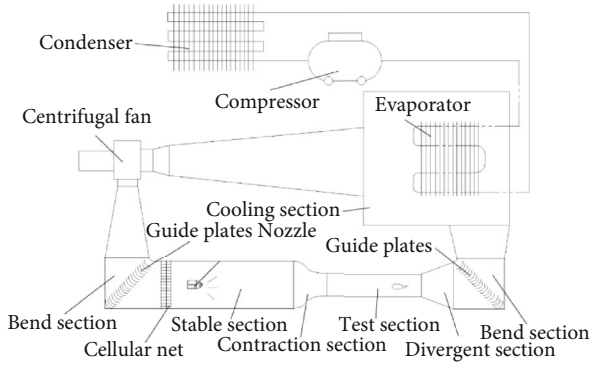

Figure 1: Principle of icing wind tunnel.

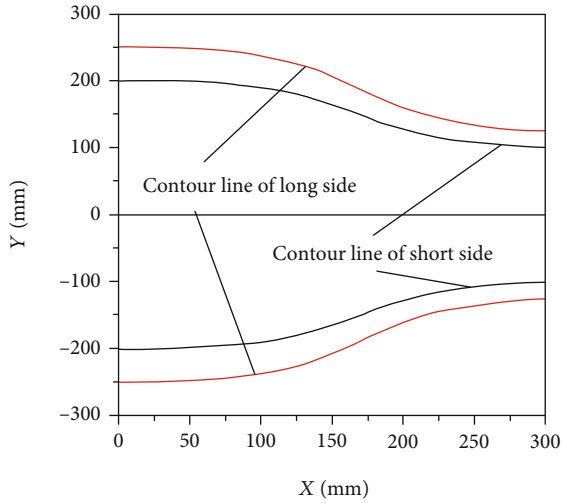

Figure 2: Curve of the contraction section.

built an open icing wind tunnel to evaluate the anti-icing performance of functional coatings by placing the channel system in a low temperature freezer. Jin and Virk [15] built a small nonreflux wind tunnel at the University of Clandfield Ice Wind Tunnel Laboratory, and carried out an ice accretion experiment on S826 and S832 wind turbine blade profiles. In summary, in addition to using a large icing wind tunnel to carry out icing research, building a small icing wind tunnel is also an important means to carry out icing and anti-icing research.

However, there are few reports on the construction of small icing wind tunnels, and only the wind tunnel construction results are given. At present, there is an icing wind tunnel built by the Technical University of Braunschweig [5], and the design, construction, and commissioning processes of the wind tunnel are introduced in detail. However, the wind tunnel structure is relatively complex, and the construction and utilization costs are high. In order to study the icing mechanism of a small model and verify the effectiveness of the anti-icing coating and deicing device, a small low-speed backflow icing wind tunnel test system is designed and built in this paper, and the design, commissioning, and test processes are described. The icing growth of typical models such as a cylinder, an NACA0018 airfoil, and an S809 airfoil is tested and compared with numerical simulation results.

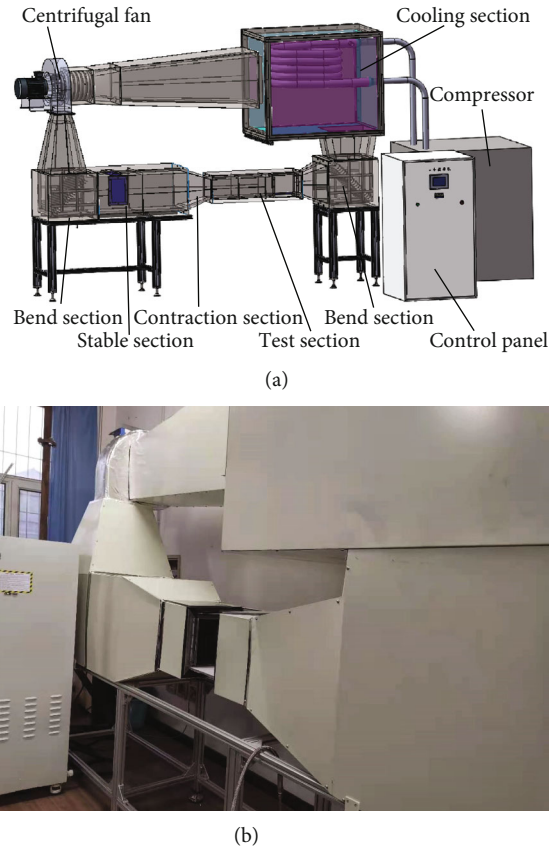

Figure 3: Modeling image and object picture of the reflux airway: (a) modeling image and (b) object picture.

The construction and utilization costs of the wind tunnel is lower, and some typical experimental cases are obtained, providing reference cases for other researchers to carry out ice shape verification.

2. Development of the Icing Wind Tunnel Experimental System

2.1. Working Principle. In this paper, the icing wind tunnel is mainly aimed at the solving the problem of small icing mechanism models, anti-icing coating performance, and deicing device effectiveness. The system is aimed at obtaining uniform velocity, uniform wind speed distribution, and controllable icing environment in the test section at low cost. Therefore, a small low-speed reflux icing wind tunnel is selected. The cross section of the wind tunnel test section is a rectangle with a dimension of250 mm × 200 mm. The designed maximum wind speed is 20 m/s. The simulated meteorological temperature range is -20°C~0°C, the liquid water content (LWC) is 0.1 g/m^3~5 g/m^3, and the medium volume diameter (MVD) of the supercooled water droplets is 20 μm~100 μm.

The schematic diagram of the small reflux icing wind tunnel is shown in Figure 1. A closed reflux duct is set up. The cooling section is arranged in the duct, and the evaporator is installed in the cooling section. The low temperature air cooled by the evaporator is pumped and pressurized by the

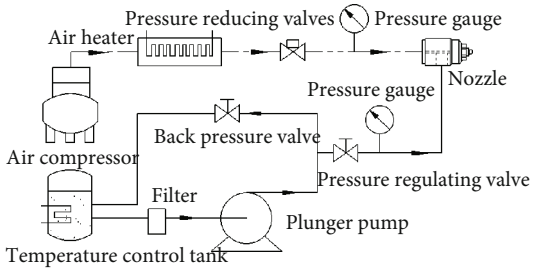

Figure 4: Spray system schematic diagram.

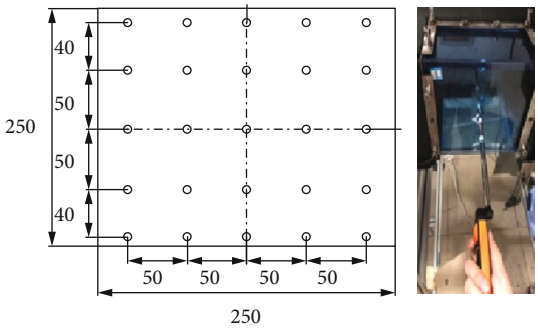

Figure 5: Position of wind speed measurement.

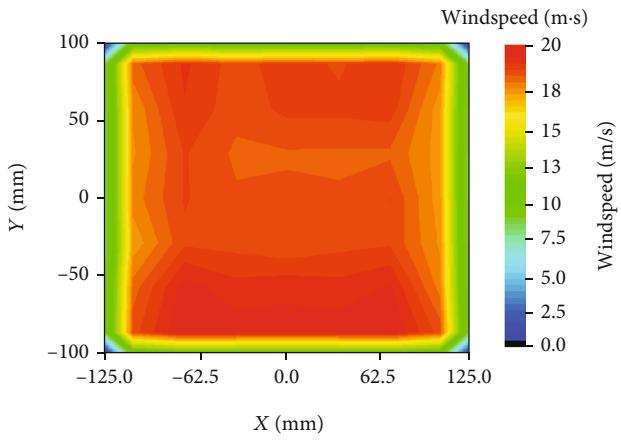

Figure 6: 18 m/s wind speed nephogram.

centrifugal fan, and then flows through the bend section. After rectification by the cellular net, it enters the stable section and the contraction section in turn. Finally, a stable airflow is formed in the test section. After the test section, it returns to the cooling section through the bend section to form a reflux. A nozzle is arranged in the stable section, and the droplet is cooled into an undercooled droplet during flight and then collides with the experimental model in the test section.

2.2. Reflux Duct. Since the cooling section is added in the return airway and the finned evaporator is installed inside, the overall aerodynamic characteristics of the reflux airway will be greatly affected. Therefore, it is unpractical to carry out aerodynamic design and analysis on all components of

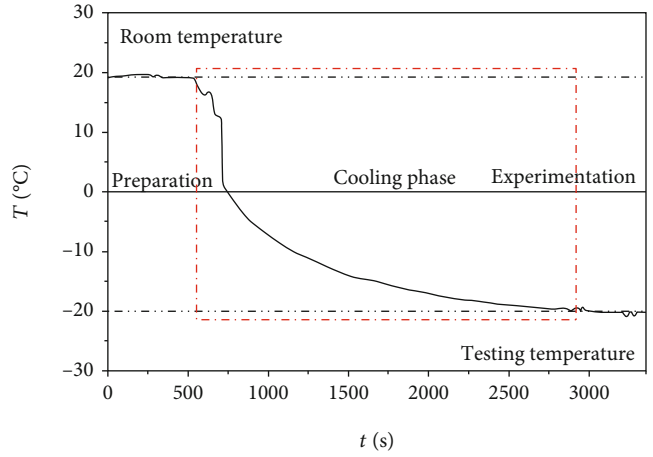

Figure 7: Curve of temperature variation.

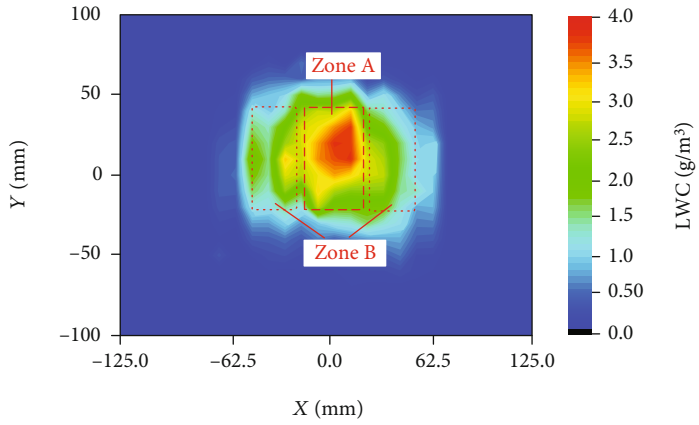

Figure 8: LWC cloud chart.

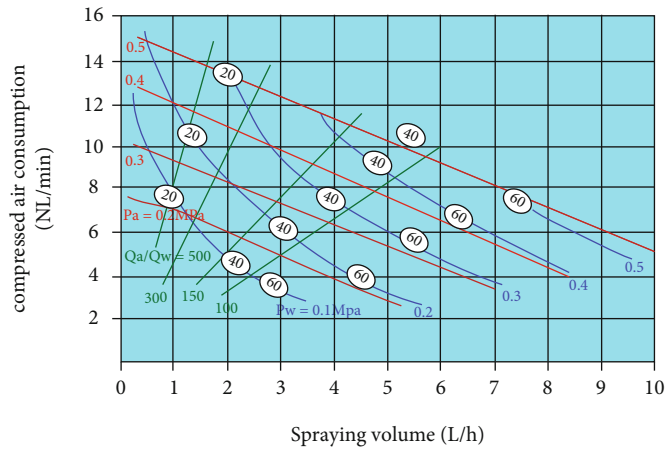

Figure 9: Characteristic curve of nozzle.

the backflow channel. We focus on the design of the flow channel from the outlet of the centrifugal fan to the inlet of the refrigerator.

The power of the reflux airway is provided by the CF-3.5-type centrifugal fan, equipped with YVF2-100S-4-type variable-frequency speed control motor with a power of

Table 1: Cylindrical icing conditions.

Contrast condition	Diameter, Φ (m)	Temperature, T (°C)	Windspeed, v (m/s)	LWC (g/m^3)	MVD (μm)	Time, t (s)
Case 1	0.03	-8	18	3.5	40	60
Case 2	0.03	-12	18	3.5	40	60
Case 3	0.03	-16	18	3.5	40	60

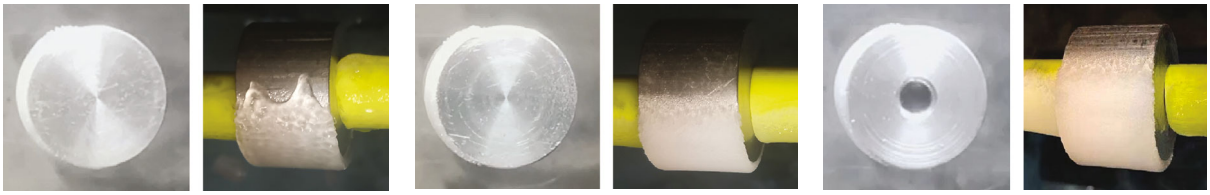

(a) (b) (c)

Figure 10: The icing types on a cylinder surface: (a) glaze ice, (b) mixed ice, and (c) rime ice.

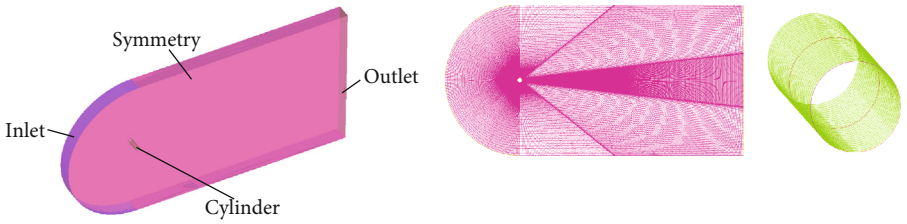

(a) (b)

Figure 11: Mesh generation of a cylinder: (a) calculated three-dimensional domain and (b) mesh.

3 kW and a constant torque frequency range of 5-50 Hz. The inlet diameter is 300 mm, and the outlet size is 250 mm × 150 mm. The outlet of the centrifugal fan is connected to the inlet of the bend section, which can convert the kinetic energy of the gas into pressure energy. Due to the insufficient conversion, the airflow will enter the bend section at a certain speed; thus, it is necessary to arrange guide plates in the bend section to improve the flow field. Both the inlet size of the bend section and the outlet size are 500 mm × 400 mm, and 19 circular arc guide plates are arranged.

The stable section is connected to the outlet of the bend section to improve the airflow uniformity and reduce the turbulence degree. At the same time, the spray droplets are fully precooled. The length of the stable section is 1000 mm, and the inlet of the spray pipe is left on the side. The entrance is equipped with a 500 mm × 400 mm cellular net. The cellular net is a hexagonal hole with a side length of 2 mm and a thickness of 10 mm. The stable section is connected to the contraction section to accelerate the airflow to reach the required speed in the test section. The inlet of the contraction section is 500 mm × 400 mm, the outlet is 250 mm × 200 mm, and the length is 300 mm. The cubic contraction curve is used. It is defined by formula (1) [16]. The actual contraction curve is shown in Figure 2.

$$\frac{D-D_2}{D_1-D_2}=\begin{cases}1-\dfrac{1}{x_m^2}\left(\dfrac{x}{L}\right)^3, \left(\dfrac{x}{L}\right)\le x_m,\\ \dfrac{1}{(1-x_m)^2}\left[1-\left(\dfrac{x}{L}\right)\right]^3, \left(\dfrac{x}{L}\right)>x_m,\end{cases} \quad (1)$$

where x_m is the connection point before and after two curves, D is the axial distance x out of the section diameter, D_1 is the shrinkage section inlet equivalent radius, D_2 is the shrinkage section outlet equivalent radius, and L is the total length of contraction section.

After the contraction section, the section size of the test section is 250 mm × 200 mm, and the length is 1000 mm. There are observation windows and test model fixing devices on it. After the test section is the diffusion section, with an outlet size of 500 mm × 400 mm and a length of 340 mm. Subsequently, the bend section was arranged to introduce the airflow into the cooling section, and 19 circular arc guide plates were arranged in the bend section. The reflux airway modeling image is shown in Figure 3(a), and the object picture is shown in Figure 3(b).

2.3. Cooling System. A Bitzer KP-4TES9Y air conditioning refrigeration compressor [17] is used in the wind tunnel refrigeration system. The compressor power is 6.62 kW, the average refrigerating capacity is 18.4 kW, and the refrigerating capacity at -20°C is 7.76 kW. The refrigerant used is R143a. The maximum cooling condition is selected to calculate the cooling capacity. At this time, the minimum operating temperature of the wind tunnel system is -20°C, and the maximum wind speed is 22 m/s. Under this condition, the energy balance equation of the wind tunnel is defined as follows:

$$Q_c = Q_s + Q_m + Q_l, \quad (2)$$

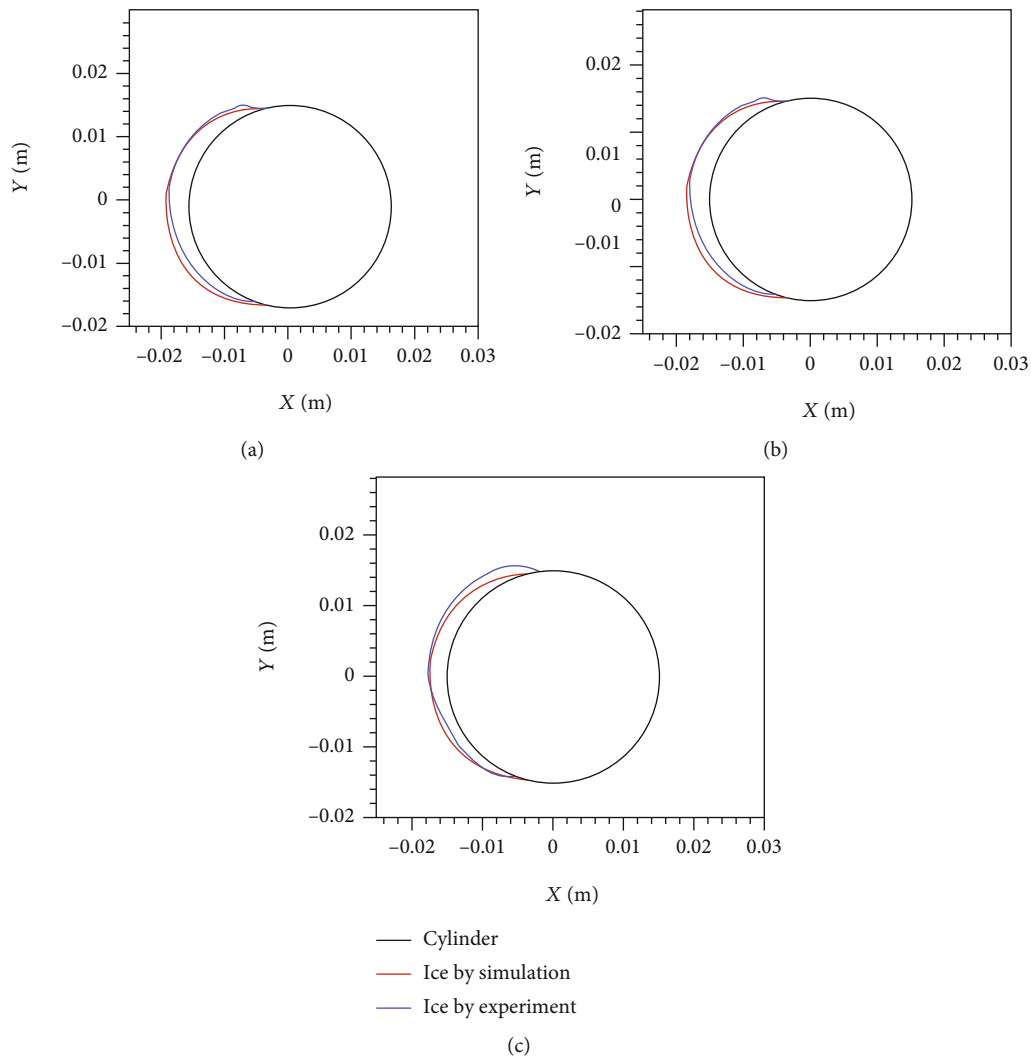

Figure 12: Icing shape comparison between test and simulation: (a) glaze ice, (b) mixed ice, and (c) rime ice.

where Q_c is the compressor refrigeration capacity, Q_s is the heat transfer by the airway and the environment, Q_m is the calorification by airflow friction, and Q_l is the heat carried away by leakage.

The heat transfer area S is calculated by the 3D model of the icing wind tunnel. The total thermal conductivity of the tunnel is defined by the following:

$$\lambda = \frac{1}{(d_1/\lambda_1 d) + (d_2/\lambda_2 d) + (d_3/\lambda_1 d)}, \quad (3)$$

where λ is the total thermal conductivity of the tunnel wall, λ_1 is the thermal conductivity of 304 stainless steel with a value of 16.3 W/m·k, λ_2 is the thermal conductivity of the rubber insulation cotton with a value of 0.034 W/m·k, d is the total thickness of the tunnel wall, d_1 is the thickness of the inner wall with a value of 2 mm, d_2 is the thickness of the rubber insulation cotton with a value of 40 mm, and d_3 is the thickness of the outer wall with a value of is 1 mm. Based on the thermal conductivity formula (3), the total thermal conductivity of the tunnel wall is 0.036 W/m·k. The heat transfer between the airway and the environment during the operation of the wind tunnel is defined by formula (4), namely, where Q_s is 0.82 kW.

$$Q_s = \frac{\lambda}{d} \cdot (T_1 - T_2) \cdot S, \quad (4)$$

where T_1 is the environmental temperature with a value of 20°C, T_2 is the testing temperature with a value of -20°C, S is the heat transfer area with a value of 24.5m^2.

The heat generated by airflow friction takes all the centrifugal fan power into heat under the limit state, namely, where Q_m is 3 kW. In the calculation, the heat absorption of water droplets increases with the increase of spray volume [8]. We take three times the wall heat transfer, where Q_l is 2.46 kW and where Q_c is 6.28 kW. This is lower than the -20°C refrigeration capacity of the compressor of 7.76 kW, which meets the refrigeration requirements.

Table 2: Symmetric airfoil icing conditions.

Contrast condition	Chord length, l (mm)	Temperature, T (°C)	Windspeed, v (m/s)	LWC (g/m^3)	MVD (μm)	Time, t (s)
Case 1	100	-8	18	3.5	40	120
Case 2	100	-12	18	3.5	40	120
Case 3	100	-16	18	3.5	40	120

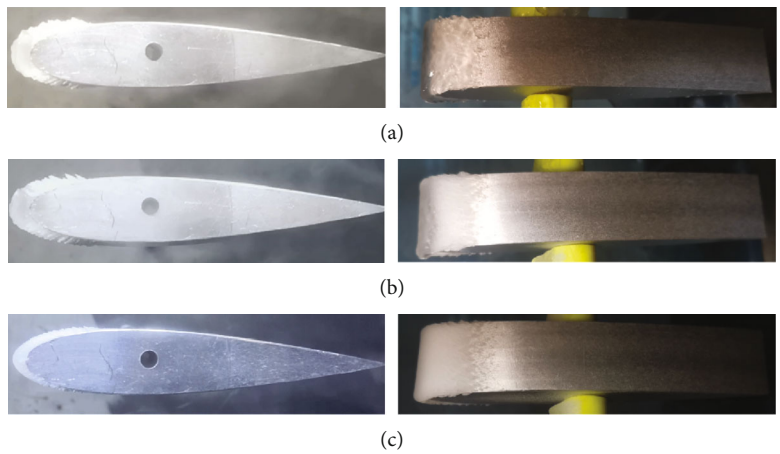

Figure 13: NACA0018 icing shape: (a) glaze ice, (b) mixed ice, and (c) rime ice.

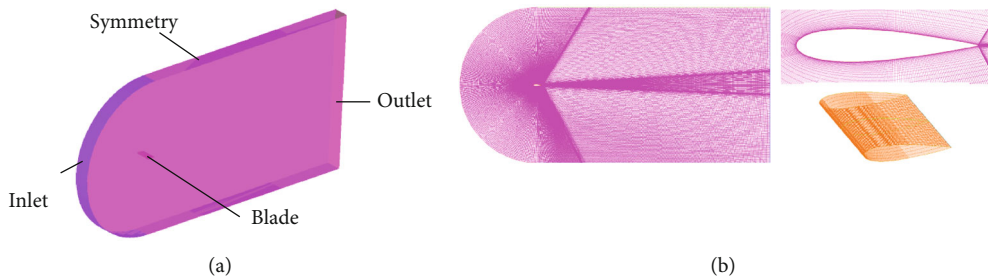

Figure 14: Mesh generation of NACA0018: (a) calculated three-dimensional domain and (b) mesh.

2.4. Spray System. The spray system adopts a two-phase flow spray, which is divided into a gas path and a water path. The pressure of the air in the gas path is adjusted by the pressure-reducing valve and preheated by the air heater before the pressure-reducing valve. The distilled water in the water channel is stored in the water tank in advance, and the temperature control system is added to the water tank to preheat the water. The water passes through the filter and enters the plunger pump to create pressure. The pressure of the water channel is adjusted by the pressure-regulating valve. Through the air heater and rectifier, water is preheated to ensure that the water and nozzle will not freeze. The spray system schematic diagram is shown in Figure 4.

The liquid water content (LWC) and the medium volume diameter (MVD) are important icing meteorological parameters, and the key is the performance of the nozzle. The system uses a CBIMJ2001 mist two-phase flow nozzle from Ikeuchi Co. Ltd., with a spray volume of 0.5 l/h~12.4 l/h and a droplet size of 20 μm~100 μm, the droplet diameter can be controlled by adjusting the pressure ratio of the gas and the liquid. With reasonable wind speed, the required icing conditions can be achieved, so we can simulate the MVD and LWC required for the freezing conditions.

3. Measurement of Meteorological Parameters of Icing Wind Tunnel

3.1. Flow Field. The wind speed of the test section under different wind speeds was measured by a hotline anemometer (model: testo 405i). The test position is shown in Figure 5. The cloud images of the test section under different wind speeds are shown in Figure 6. It can be seen that the wind speed is uniform, which meets the test requirements.

3.2. Temperature. The cooling process of the test section is tested by a hot-wire anemometer. The temperature change at the center of the test section during a certain test process is shown in Figure 7. The temperature at the initial stage is

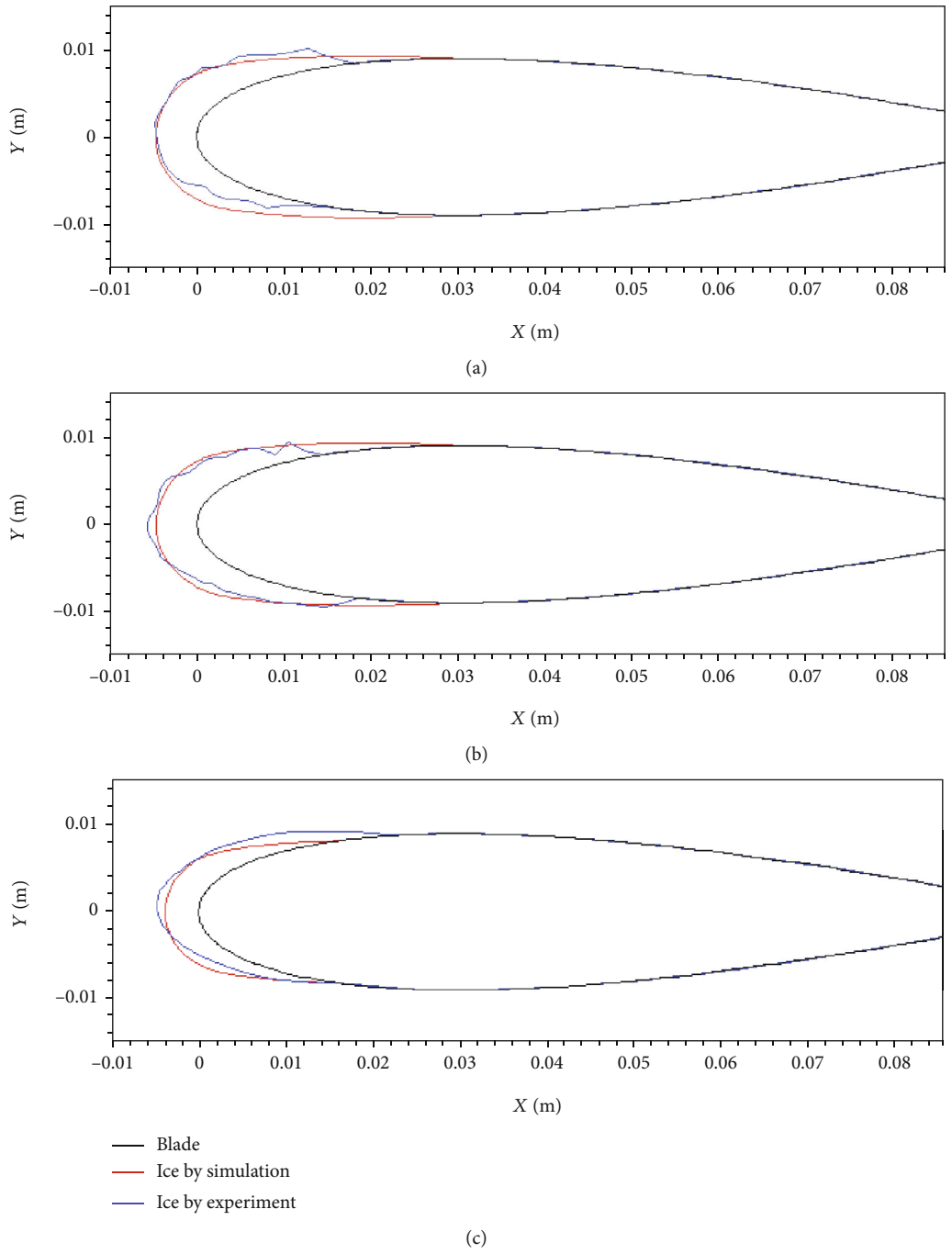

Figure 15: Ice shape comparison of NACA0018 icing: (a) glaze ice, (b) mixed ice, and (c) rime ice.

the same as that at room temperature. When the centrifugal fan is opened to make the air circulate in the duct, the refrigeration device is opened. The temperature of the test section begins to decline. When the temperature drops to the preset temperature of -20°C, it remains constant. It can be seen that the wind tunnel can meet the needs of the refrigeration system.

3.3. LWC and MVD. The LWC in the test section was measured by the ice knife method [18]. The ice knife was 200 mm in length, 20 mm in width, and 3 mm in thickness, and the material was stainless steel. According to the references, the ice thickness is controlled between 1.6 mm and 4.5 mm, the ice width is kept at less than 5 mm, and the distribution of liquid water content is based on the following formula:

$$\mathrm{LWC} = \frac{\rho_{\mathrm{ice}} \times h_i}{v}, \tag{5}$$

Table 3: Asymmetric airfoil icing conditions.

Contrast condition	Chord length, l (mm)	Temperature, T (°C)	Windspeed, v (m/s)	LWC (g/m^3)	MVD (μm)	Time, t (s)
Case 1	100	-8	18	3.5	40	120
Case 2	100	-12	18	3.5	40	120
Case 3	100	-16	18	3.5	40	120

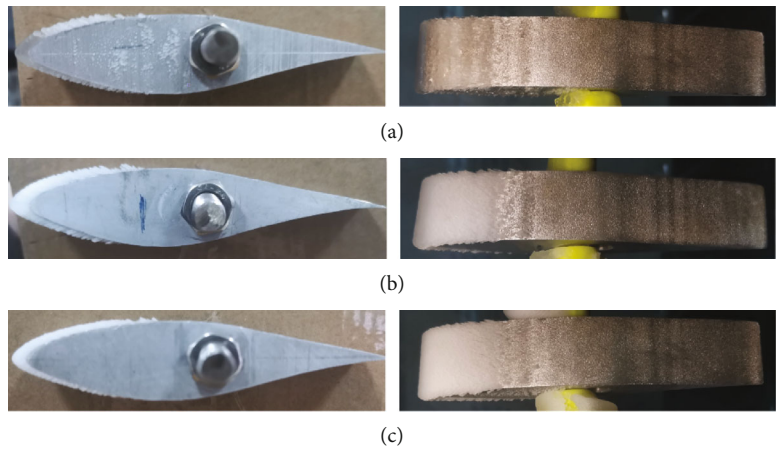

Figure 16: S809 icing shape: (a) glaze ice, (b) mixed ice, and (c) rime ice.

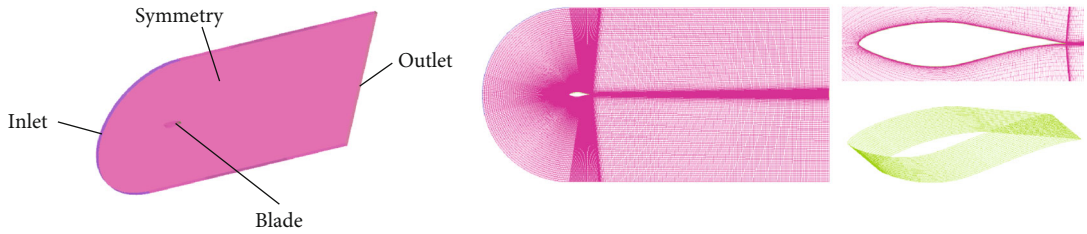

Figure 17: Mesh generation of S809: (a) calculated three-dimensional domain and (b) mesh.

where ρ_{ice} is the ice density (at 720 kg/m^3), h_i is the ice thickness on the ice knife, v is the wind speed in the test section.

The obtained LWC distribution nephogram on the cross section of the test section at 18 m/s wind speed is shown in Figure 8, it can be found that the spray has a certain degree of inhomogeneity due to the influence of the nozzle's own properties. Zone A and Zone B are distinguished. The liquid water content of the spray in Zone A is 0.35 g/m^3, and that in Zone B is 0.2 g/m^3. The models used in this experiment were all carried out in Zone A to adapt to the spray inhomogeneity. According to the inherent spray characteristics of the nozzle, as shown in Figure 9, the medium volume diameter (MVD) of the spray can be calculated to be 40 μm based on the spray amount of the nozzle.

4. Icing Wind Tunnel Test Performance Verification

The icing wind tunnel was used to test the cylinder, the symmetrical airfoil NACA0018 blade section, and the asymmetric airfoil S809 blade section under glaze ice, mixed ice, and rime ice conditions.

4.1. Cylinder Icing Test. The selected cylindrical model is made of aluminium with a diameter of 0.03 m and a thickness of 0.02 m. In each experiment, the test system needs to be calibrated to determine the nozzle water spraying amount. The installation position and spray angle are consistent with the calibration of meteorological parameters. The air duct was precooled by opening the refrigeration system, and the uniformity of LWC was checked again by ice knife. After the wind tunnel debugging, the test model was installed in the test section. Before icing spray, the airway and test model should be fully precooled to ensure the temperature consistency of the whole test system. The precooling time was at least 3 min. After the icing condition is completed, the spray system is closed to keep the airway in a low temperature state. The experiment is completed after the two-dimensional image of icing is collected by CCD camera [19]. Each group of tests

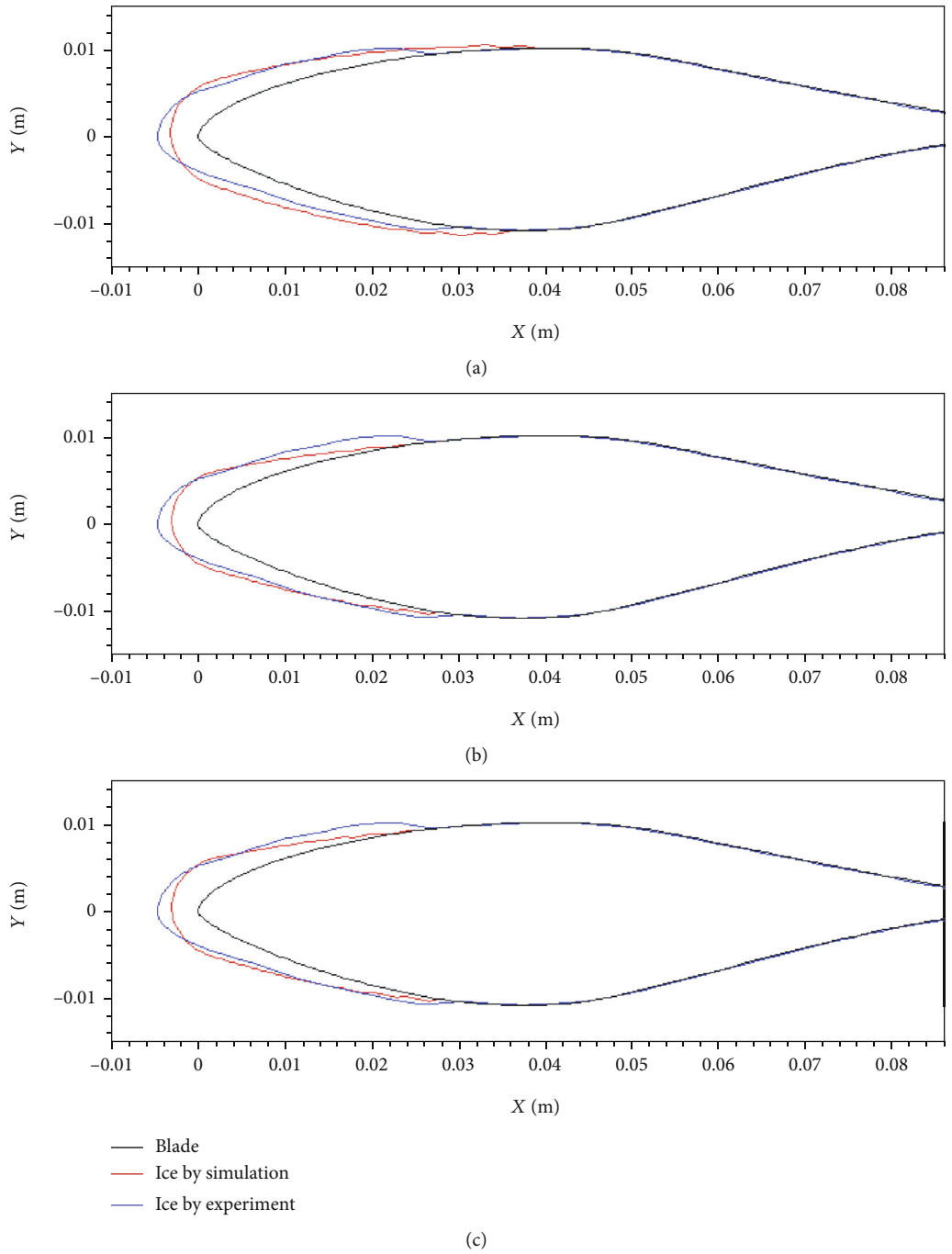

Figure 18: Ice shape comparison of S809 icing: (a) glaze ice, (b) mixed ice, and (c) rime ice.

should be repeated more than three times to ensure the consistency of the test results.

Table 1 is the test medium volume diameter conditions. Figure 10 shows the test results. It can be found that the corresponding working condition Case 1 in Figure 10(a) is glaze ice icing. From the side pictures, it can be seen that the icing is transparent and the ice ridge appears. Figure 10(b) is Case 2 for mixed ice, and Figure 10(c) is Case 3 for rime ice. From the side diagram, it can be seen that mixed ice is combined with glaze ice while rime ice is not, and the ice shape is slightly larger than that of glaze ice.

In order to further verify the accuracy of the system, the obtained two-dimensional ice shapes had been compared with the icing ice shapes which were calculated by the numerical simulation software FENSAP-ICE [20]. ICEM is used for mesh generation, and the calculated three-dimensional domain and mesh are shown in Figure 11. The flow field around the model is simulated by the FENSAP Solver, and

the air flow field is solved by the N-S equation with viscous calculation and analysis. The turbulence model is the k-omega SST model. The water droplet trajectory is solved in the DROP3D Solver, and the solution model is the Eulerian two-fluid model. Simulation of an ice shape was conducted in the ICE 3D Solver by the improved Messinger thermodynamic model.

The ice shape obtained is shown in Figure 12. It can be found that the trend of the ice shape is roughly the same. In the rime ice state, the coincidence degree is particularly higher. In the glaze ice state, the coincidence degree is slightly worse, which is due to the occurrence of ice ridges leading to a partial deformation of the ice.

4.2. Symmetric Blade Airfoil Icing Test. The airfoil is NACA0018, and the material is aluminium. The chord length c is 0.1 m, and the thickness is 0.02 m. The test process is the same as that of cylinder icing, and the test scheme is shown in Table 2. The ice shape obtained is shown in Figure 13. In Figure 13(a), the corresponding Case 1 is glaze ice, and there is no uniform distribution of ice at the edge of the icing. Figures 13(b) and 13(c) correspond to Case 2 and Case 3, respectively, which are mixed ice and rime ice.

The obtained two-dimensional ice shape is compared with the ice shape of the numerical simulation software FENSAP-ICE. Mesh generation is shown in Figure 14, and the calculation method is the same as that of cylinder icing.

As shown in Figure 15, it can be found that the trend of the ice shape is roughly the same, and the coincidence degree is higher in the rime state. In the glaze ice and mixed ice states, the ice shape coincidence is slightly worse due to the formation of a nodular structure. Overall, the experimental ice shape has a high coincidence degree with the calculated ice shape.

4.3. Asymmetric Blade Airfoil Icing Test. The typical airfoil S809 was selected for the icing test. The material is aluminium, the chord length c is 0.1 m, and the thickness is 0.02 m. The test process is the same as that of cylinder icing, and the test scheme is shown in Table 3. The glaze ice obtained under Case 1 is shown in Figure 16(a). There is no nodular ice on the upper surface of the airfoil, which has the characteristics of partially mixed ice. Case 2 and Case 3 are mixed ice and rime ice, respectively. As shown in Figures 16(b) and 16(c), rime ice features are more obvious, and the mixed ice is mainly manifested at the leading edge, which is due to the difference in the heat transfer caused by the different aerodynamic characteristics of S809 and NACA0018.

The obtained two-dimensional ice shape is compared with the ice shape of the numerical simulation software FENSAP-ICE. Mesh generation is shown in Figure 17, and the calculation method is the same as that of cylinder icing. As shown in Figure 18, it can be found that the trend of the ice shape is roughly the same, which intersects with NACA0018. The ice shape overlap is slightly worse when the asymmetric airfoil is icing, and the leading edge of the ice shape is sharper.

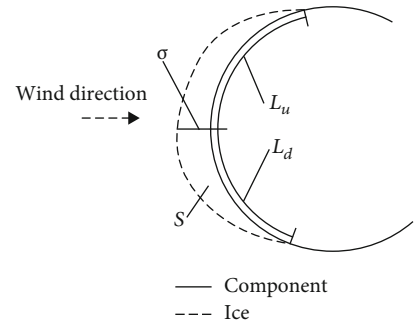

Figure 19: Typical characteristic quantities.

5. Analysis of Icing Overlap Characteristic Quantity

In order to study the similarity degree of the ice shape more intuitively, the irregular ice shape is analyzed quantitatively and the typical characteristic quantity is determined to evaluate the obtained two-dimensional ice shape [19]. As shown in Figure 19, the icing area is s, the icing thickness is σ, the icing upper limit is L_u, and the icing lower limit is L_d. They are selected to evaluate the coincidence degree of icing through the difference rate, where the e-subscript represents the test data and the s-subscript represents the calculation data.

Here, the area difference rate is as follows:

$$\xi_S = \left|\frac{(S)_e - (S)_s}{(S)_e}\right|, \tag{6}$$

where, the leading-edge thickness difference rate is as follows:

$$\xi_\sigma = \left|\frac{(\sigma)_e - (\sigma)_s}{(\sigma)_e}\right|, \tag{7}$$

where, the ice superior limit difference rate is as follows:

$$\xi_{L_u} = \left|\frac{(L_u)_e - (L_u)_s}{(L_u)_e}\right|, \tag{8}$$

where, the ice inferior limit difference rate is as follows:

$$\xi_{L_d} = \left|\frac{(L_d)_e - (L_d)_s}{(L_d)_e}\right|. \tag{9}$$

The influence weight r_i of different typical characteristic quantities are defined. Because the icing area and leading-edge thickness can better reflect the icing difference, the weight of the icing area r_S is 0.3, the weight of the leading-edge thickness r_σ is 0.3, the limit weight of the icing r_{L_u} is 0.2, and the limit weight of icing r_{L_d} is 0.2, that is, the overall difference of the ice shape is as follows:

$$\begin{aligned} \text{Sim} &= \left[1 - \left(\xi_S r_S + \xi_\sigma r_\sigma + \xi_{L_u} r_{L_u} + \xi_{L_d} r_{L_d}\right)\right] \\ &= \left[1 - \left(0.3\xi_S + 0.3\xi_\sigma + 0.2\xi_{L_u} + 0.2\xi_{L_d}\right)\right]. \end{aligned} \tag{10}$$

Table 4: Asymmetric airfoil icing conditions.

	Cylinder			NACA0018			S809		
	Glaze ice	Mixed ice	Rime ice	Glaze ice	Mixed ice	Rime ice	Glaze ice	Mixed ice	Rime ice
Sim	67.8%	87.5%	90.1%	70.5%	71.1%	83.7%	72.7%	76.0%	80.9%

Table 4 shows the similarity between the experimental ice shape and the numerical simulation ice shape. The results show that in the rime ice state, the icing similarity of the cylinder, the symmetric airfoil, and the asymmetric airfoil is high, and the highest cylinder reaches 90.1%, while the differences of the airfoil are 83.7% and 80.9%, respectively. The overlap degree of the mixed ice and the glaze ice is slightly worse, and the overlap degree of the ice shape is about 70% in the open ice state. The reasons for the observations above are not only because the conventional icing numerical simulation cannot completely reproduce the actual icing conditions but also because the working conditions in this paper are all carried out at low Reynolds numbers, and the inflow wind speed is only 18 m/s. During the icing process, a certain degree of settlement occurs during the droplet flight, which leads to the difference in icing shape, which also indicates the necessity of an icing wind tunnel test. In summary, the development trend of icing is roughly the same, which can reflect the actual icing situation. The system can meet the experimental requirements of icing research on a blade model.

6. Conclusions

In order to study the icing of a wind turbine more conveniently, a small reflux type low-speed icing wind tunnel test system is designed and built. The conclusions are as follows:

(1) After the overall structure of the wind tunnel was determined, the reflux airway, the refrigeration system, and the spray system were designed. After the wind tunnel was built, the flow field distribution, the temperature stability, and the liquid water content (LWC) distribution of the three typical environmental variables of the test system were measured and analyzed. The measurement and analysis of icing wind tunnel meteorological parameters are obtained through many tests. The results show that the test system has good repeatability and stable performance

(2) Ice test was carried out by using the cylindrical model and the blade model, and the ice shape obtained by the test was compared with that obtained by a commercial numerical simulation software. The coincidence degree of an irregular ice shape is evaluated by icing overlap characteristic quantity. The results show that the coincidence degree of the icing ice shape is higher in the rime ice state and slightly worse in the glaze ice state. Overall, the development trend of icing is roughly the same, which can reflect the actual icing situation. The system can meet the test requirements of blade model icing research

Data Availability

The data used to support the findings of this study are included within the article.

Conflicts of Interest

The authors declare that there are no conflicts of interest regarding the publication of this paper.

Acknowledgments

This research is supported by the National Natural Science Foundation of China (NSFC, No. 51976029) and the State Key Laboratory of Alternate Electrical Power System with Renewable Energy Sources (Grant No. LAPS19007).

References

[1] Y. Zhao, Q. Guo, T. Lin, and P. Cheng, "A review of recent literature on icing phenomena: transport mechanisms, their modulations and controls," *International Journal of Heat and Mass Transfer*, vol. 159, p. 120074, 2020.

[2] Z. Wang, C. Zhu, and N. Zhao, "Experimental study on the effect of different parameters on rotor blade icing in a cold chamber," *Applied Sciences*, vol. 10, 2020.

[3] V. A. Sergey and A. P. Oleksander, "Numerical simulation of icing of a cylinder and an airfoil: model review and computational results," *TsAGI Science Journal*, vol. 44, 2013.

[4] P. J. Jordaens, A. Krenn, M. Wadham-Gagnon, N. Davis, and R. Cattin, *IEA Wind Task 19—Available Technologies Report of Wind Energy in Cold Climates*, 2016.

[5] S. E. Bansmer, A. Baumert, S. Sattler et al., "Design, construction and commissioning of the Braunschweig icing wind tunnel," *Atmospheric Measurement Techniques*, vol. 11, no. 6, pp. 3221–3249, 2018.

[6] J. F. Vanzante, R. F. Ide, and L. E. Steen, "NASA Glenn Icing Research Tunnel: 2012 cloud calibration procedure and results," in *4th AIAA Atmospheric and Space Environments Conference*, New Orleans, Louisiana, USA, 2012.

[7] C. Clark and M. MacMaster, "Icing wind tunnel tests of a contaminated supercritical anti-iced wing section during simulated take-off—phase 2," in *4th AIAA Atmospheric and Space Environments Conference*, New Orleans, Louisiana, USA, 2012.

[8] D. Hammond, "Cranfield University Icing Wind Tunnel," *Aerospace Sciences Meeting & Exhibit*, 2013.

[9] G. Linyue, L. Yang, M. Liqun, and H. Hui, "A hybrid strategy combining minimized leading-edge electric-heating and superhydro-/ice-phobic surface coating for wind turbine icing mitigation," *Renewable Energy*, vol. 140, 2019.

[10] F. Zhang, L. Zhang, Y. Li, Z. Liu, and P. Zhu, "Experimental investigation of the icing scaling test method for a rotating cone," *Proceedings of the Institution of Mechanical Engineers*, vol. 233, 2019.

[11] C. X. Zhu, C. L. Zhu, W. W. Zhao, and M. J. Tao, "Experimental study on the shear adhesion strength between the ice and substrate in icing wind tunnel," *Journal of Mechanics*, vol. 34, pp. 209–216, 2018.

[12] G. Joseph, K. Daiki, M. Tetsuro et al., "Novel superhydrophobic surface with solar-absorptive material for improved deicing performance," *Materials*, vol. 12, 2019.

[13] D. De Pauw and A. Dolatabadi, "Effect of superhydrophobic coating on the anti-icing and deicing of an airfoil," *Journal of Transportation*, vol. 54, no. 2, pp. 490–499, 2017.

[14] J. R. Pedro, J. R. Rafael, L. Silvia et al., "Evaluation of functionalized coatings for the prevention of ice accretion by using icing wind tunnel tests," *Coatings*, vol. 10, 2020.

[15] Y. J. Jia and S. V. Muhammad, "Experimental study of ice accretion on S826 & S832 wind turbine blade profiles," *Cold Regions Science And Technology*, vol. 169, 2020.

[16] T. Morel, "Comprehensive design of axisymmetric wind tunnel contractions," *ASMEPaper 75-FE-17*, 1975.

[17] *BITZER KP-4TES9Y air conditioning refrigeration compressor's parameter table*2019 pageshttps://www.bitzer.de/gb/en/reciprocating-compressors/ecoline/#!4TES9.

[18] R. Idea, "Liquid water content and droplet size calibration of the NASA Lewis Icing Research Tunnel," in *28th Aerospace Sciences Meeting*, 669 pages, Reno, NV, USA, 1990.

[19] L. Yan, S. Ce, J. Yu, and F. Fang, "Scaling method of the rotating blade of a wind turbine for a rime ice wind tunnel test," *Energies*, vol. 12, 2019.

[20] G. M. Ibrahim, K. Pope, and Y. S. Muzychka, "Effects of blade design on ice accretion for horizontal axis wind turbines," *Journal of Wind Engineering & Industrial Aerodynamics*, vol. 173, 2018.